Physics of Plasmas ARTICLE scitation.org/journal/php

Generation of supersonic jets from underwater electrical explosions of wire arrays

Cite as: Phys. Plasmas **28**, 063509 (2021); doi: 10.1063/5.0050430
Submitted: 16 March 2021 · Accepted: 10 May 2021 ·
Published Online: 9 June 2021

D. Maler,[1,a)] S. Efimov,[1] A. Rososhek,[1] S. N. Bland,[2] and Ya. E. Krasik[1]

AFFILIATIONS

[1]Physics Department, Technion, Haifa 32000, Israel
[2]Plasma Physics Group, Imperial College London, London SW7 2BW, United Kingdom

[a)]Author to whom correspondence should be addressed: daniel.maler@campus.technion.ac.il

ABSTRACT

Underwater electrical explosion experiments of cylindrical or conical wire arrays accompanied by the generation of fast (up to ∼4500 m/s) water jets are presented. In these experiments, a pulse generator with a stored energy of up to ∼5.7 kJ, current amplitude of up to ∼340 kA, and rise time of ∼0.85 μs was used to electrically explode copper and aluminum wire arrays underwater. Streak and fast framing shadow imaging was used to extract the space–time resolved velocity of the ejected jet from the array while it propagates in air. The jet generation occurs due to high pressure and density of water formed in the vicinity of the array axis by the imploding shockwave. It was shown that the velocity of the jet ejected from the array depends on the array geometry and the thickness of the water layer above the array. The results suggest that ≥50% of the energy deposited into the array is transferred to the kinetic energy of this jet and the axial waterflow.

I. INTRODUCTION

The study of matter at extreme pressures and densities, the subject of High Energy Density Physics (HEDP), is of great importance to basic physics, in astrophysics, and for different practical applications.[1–4] Laboratory studies of such conditions need energy densities of 10–100 kJ/cm^3 which can be provided by a variety of drivers, such as Z-pinch,[5] plasma focus,[6] powerful pulsed laser systems,[7] multistage gas guns,[8] high energy heavy ion beams,[9] and chemical explosives.[1]

Research of underwater electrical explosion of wires demonstrated that this approach can also be applied for HEDP studies[10,11] using pulsed power generators with a stored energy of several kJ. It was shown that the underwater electrical explosion of a wire is characterized by an efficient (up to 24%) transfer of the energy deposited in the wires into a generated shockwave (shock) and the subsequent waterflow behind the shock front.[12,13] Studies have shown that for cylindrical or spherical wire array explosions, the converging shocks produce extremely high pressures (≥10^{11} Pa), densities (≥2 g/cm^3), and temperature (≥ 2 eV) in the water.[14,15]

For more than 80 years, the behavior of underwater explosive charges, the generation of strong shocks from these, and the production of water jets have been studied experimentally and theoretically in civil and defense applications.[16–18] In experiments with ∼10 kg of explosives, jets with velocities reaching ∼2500 m/s were formed by a cavitation phenomenon in the vicinity of the water–air boundary. In pulsed power driven experiments with underwater conical wire arrays, water jets with velocities reaching ∼1250 m/s were demonstrated.[19] For these experiments, assuming steady state radial pressure distribution and considering the radially converging waterflow in the acoustic approximation, a simplified model was suggested to explain the jet generation inside cones within a specific range of angles. Using a fitting parameter for the efficiency of the energy transfer to the waterflow, the results of this model were in satisfactory agreement with the observed jet velocity, which in the frame of this model was estimated to be less than 1500 m/s. On the other hand, this model failed to explain possible jet generation for cylindrical arrays.

In the present paper, we use the same pulsed power generator with stored energy of ≤5.7 kJ as in our earlier study,[19] but with significantly improved time- and space-resolved optical diagnostics. In addition, we employ a new design of the cylindrical array such that it significantly reduces the thickness of the water layer between the exploding wires and the water–air interface, which was not considered in previous work. Due to this new design, we measure water jet velocities of up to ∼4000 m/s for underwater exploding cylindrical arrays while for conical arrays, velocities reaching ∼4500 m/s were attained. The results of this research demonstrate that underwater electrical explosions are a promising approach for the generation of high energy jets without high explosives.

II. EXPERIMENTAL SETUP AND DIAGNOSTICS

The experimental setup and the diagnostics are shown in Fig. 1. A pulse generator[20] supplied to the wire array current pulses with a typical rise time of ~0.85 μs and amplitudes of $\leq$270 kA or $\leq$340 kA when charged to φ_{ch} = 27 kV (stored energy of ~3.8 kJ) and φ_{ch} = 33 kV (stored energy of ~5.7 kJ), respectively. A calibrated self-integrating Rogowski coil and a P6015 Tektronix voltage divider were used to measure the waveforms of the discharge current I and the voltage V applied to the array.

In experiments, 40 mm long, cylindrical (5 or 10 mm diameter) and truncated cone arrays, each made of 40 copper wires, were tested. A critically damped discharge, where most of the energy stored in the capacitors is transferred to the array during a time comparable with the quarter period of an under-damped discharge, was obtained for copper wires of 100 and 114-μm diameter for φ_{ch} = 27 and φ_{ch} = 33 kV, respectively. In several experiments, performed at φ_{ch} = 33 kV, arrays consisting of 40 aluminum wires, each of 150-μm diameter, were used. The array was placed in a stainless-steel chamber, filled with de-ionized water, with Perspex windows for optical observations (see Fig. 1). For conical arrays, the high voltage electrode has a hole with a diameter of 5 mm, and the ground electrode has a hole with a diameter of either 15 mm (apex angle of 7.12°) or 10 mm (apex angle of 3.57°). The 1-mm thick grounded electrode was submerged under water. The wires were soldered to the upper surface of the electrode, and the height of the water layer, noted as h_w, was varied in the range 2–14 mm (see Fig. 1). In some experiments, a 1-mm thick stainless-steel disk (referred to as collimator), with a 2-mm lower diameter and 5-mm upper diameter conical hole (see Fig. 1), was used. The collimator allowed decreasing the thickness of the water level to 1 mm.

The light emission from the water in the vicinity of the implosion axis ($r < 0.5$ mm) was observed by an optical fiber coupled with a Hamamatsu R7400U-04 photo-multiplier tube (PMT). The fiber was installed inside a 1-mm-diameter capillary placed at ~15 mm from the water level. It was shown in the earlier research of cylindrical wire explosions[11] that the shock convergence leads to an increase in the temperature of compressed water to several eV in the vicinity of the axis. Thus, the shock time-of-flight (TOF) was calculated as the time delay between the beginning of the light emission registered by the PMT and the maximum of the deposited power.

A diode-pumped continuous wave (CW) single-mode laser (~1.5 W, λ = 532 nm) was used to backlight the waterflow and the jet emerging from the array and the shock generated in air. Shadow images of the upstream ejected waterflow and jet were obtained using two 4QuickE ICCD cameras (Stanford Computer Optics Inc.) operating with a frame exposure time of 5 ns. In some experiments, we set the cameras to capture a sequence of two frames, obtained with 1 μs time delay, thus producing overlapping images. Using spatial calibration for each 4QuickE camera, the height of the jet was calculated relative to the initial water level. The time delay between each image was measured relative to the beginning of the discharge current. Thus, the waterflow, V_w, and jet velocity, V_j, were calculated within the error of $\pm$150 m/s, using the height difference between successive images and the time delay between images. This error originates from the smearing ($\pm$3 pixels) of the waterflow and the jet front. Assuming that the jet generation starts approximately at the time when the shock reaches the axis, the maximal average jet velocity (referred to as estimated jet velocity), V_j^*, was estimated as: $V_j^* = h_j/(t - \Delta t_l)$ using the first shadow frame image, where the jet was obtained at time t and distance h_j relative to the location to the array's grounded electrode . t and Δt_l are the time delays of the frame and the light emission peak relative to the beginning of the discharge current, respectively. Here let us note that in the case of conical array explosion, instead of light emission peak, only a smooth (tens of ns rise time) increase in light intensity was obtained at the time when the shock is expected to reach implosion axis. Thus, for these explosions the value of Δt_l was considered equal to that obtained for a cylindrical array. The latter does not lead to significant error in estimation of V_j^* because the uncertainty of $\pm$0.1 μs in Δt_l would result in uncertainty $\pm$300 m/s in value of V_j^*. In addition, the jet and waterflow trajectories were obtained using a streak Optoscope SC-10 camera (Optronis GmbH). The camera slit, set to a width of 200 μm, was positioned in the perpendicular direction

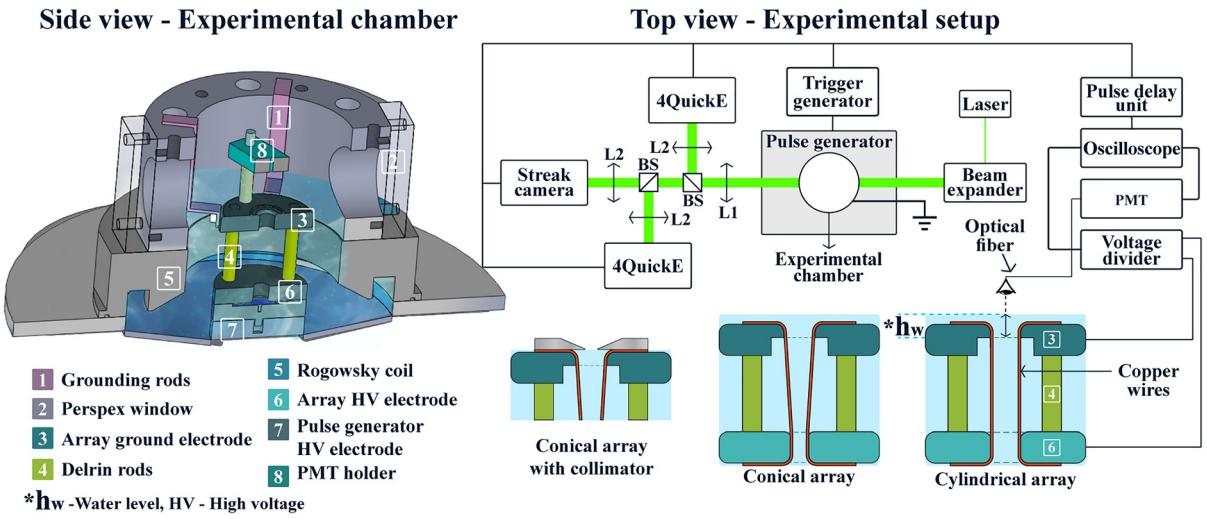

FIG. 1. Experimental setup and diagnostics.

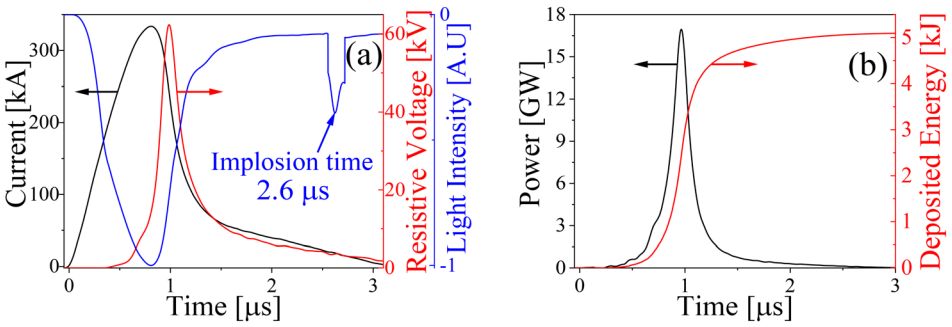

FIG. 2. Waveforms of the discharge current, resistive voltage, and PMT signal (a) and the calculated deposited power and energy (b) for a 10 mm diameter cylindrical wire array, at $\varphi_{ch} = 33$ kV.

relative to the cone base and was adjusted to view the cone axis. The error in the velocity calculation using the streak images is estimated as ±150 m/s. However, the axial position of the camera slit, in many shots, did not coincide with the axis of the jet which, as it will be shown below, was <0.8 mm wide, which raises questions with respect to the accuracy of the estimated jet velocity.

Typical waveforms of the discharge current, I, resistive voltage, V_{res}, light emission intensity, deposited power, and energy for an explosion of a 10 mm diameter cylindrical wire array at $\varphi_{ch} = 33$ kV are presented in Fig. 2. The inductive voltage $L\frac{dI}{dt}$, where the wire array inductance $L \sim 20$ nH, was subtracted from the measured value of the voltage to obtain the value of V_{res}. The wire array inductance was estimated in shots with a short-circuit load simulating the array. One can see that the discharge is almost critically damped and that the amplitude of the discharge current reaches ~340 kA within ~0.85 μs and almost 75% (~4 kJ) of the stored energy is deposited into the wire array within ~0.7 μs. Similar critically damped discharges were obtained for conical wire arrays and for $\varphi_{ch} = 27$ kV. In the latter, the amplitude of the discharge current was ~270 kA and the deposited energy ~3 kJ. In Fig. 2(a), one can also see a ~100-ns-long spike in the PMT waveform, which is related to the light emission of the water plasma formed by the converging shock in the vicinity of the axis.[11] These data were used to estimate the time-of-flight of the converging shock, which is generated with the sharp decrease in the discharge current.

III. EXPERIMENTAL RESULTS

A. Generation of waterflow and jets by cylindrical wire array explosions

The explosions of arrays were accompanied by emerging waterflow and a narrow high-speed water jet, propagating along the symmetry axis, whose velocities were found dependent on h_w, d_{ar}, and φ_{ch}. In this set of experiments, carried out at 27 and 33 kV charging voltages, we used cylindrical arrays with diameters, d_{ar}, of 10 and 5 mm. Experiments were conducted with different water levels, h_w, varied in the range 1–14 mm above the array (see Fig. 1). The accuracy of the initial water level measurement, performed using an optical system and a calibrated rule, was ±0.1 mm.

1. Waterflow parameters from cylindrical arrays

Our measurements indicate that as the height of the water level is decreased, the average velocity of the waterflow significantly increases. Namely, for explosions of a $d_{ar} = 10$ mm array diameter at $\varphi_{ch} = 27$ kV, the average flow velocities, V_w, were ~350, ~400, and ~550 m/s, for h_w values of 14, 10, and 5 mm, respectively. With higher charging voltages, and even smaller h_w this velocity continued to increase, i.e., at $\varphi_{ch} = 33$ kV we obtained $V_w = \sim 700$, ~900, ~1400, and ~2500 m/s, for $h_w = 5$, 3, 2, and 1 mm, respectively. This behavior is due to smaller water mass being accelerated by the pressure build-up inside the array resulting from the converging shock, accompanied by the waterflow behind its front and the radial expansion of the wires. The extremely high velocity value, obtained when $h_w = 1$ mm, can be related to the formation of a plasma in a thin water layer due to the explosion of the wires, which are soldered to the ground electrode (see Fig. 1). This assumption is qualitatively confirmed by bright light spots seen in Fig. 3(a) in the waterflow when $h_w = 1$ mm.

Next, the value of V_w was measured for an array with $d_{ar} = 5$ mm, at $\varphi_{ch} = 27$ kV and with $h_w = 14$ mm. In these experiments, the waterflow velocity was measured to be $V_w \sim 550$ m/s, faster compared to explosions carried out with $d_{ar} = 10$ mm. For $\varphi_{ch} = 33$ kV, $d_{ar} = 5$ mm, and $h_w = 2$ mm, the flow velocity was $V_w \sim 1350$ m/s, only slightly smaller than the waterflow velocity obtained for $d_{ar} = 10$ mm at the same water level. The shapes of the waterflow however were very different for $d_{ar} = 10$ and 5 mm at the same charging voltage and water level (see Fig. 4). In the case of $d_{ar} = 10$ mm [Fig. 4(b)], the axial waterflow surface is almost flat, whereas for the case of $d_{ar} = 5$ mm [Fig. 4(a)], it is parabolic. These results can be related to the space–time evolution of the flow. Namely, the axial flow starts at a larger radius for larger d_{ar}, where the pressure of the converging waterflow is smaller than for smaller d_{ar} and the axial flow's development is delayed. This non-instantaneous temporal and spatial development of the axial waterflow leads to a time varying shape of the front of the flow. Thus, qualitatively, one can expect that for explosions with $d_{ar} = 5$ mm, characterized by a higher energy-density deposition into the radial waterflow, the axial waterflow generated at smaller radii,

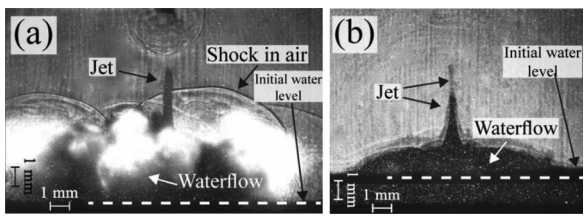

FIG. 3. Shadow images of the waterflow and jet obtained in shots with $d_{ar} = 5$ mm, $h_w = 1$ mm, and $t = 6$ μs (a) and $d_{ar} = 10$ mm, $h_w = 2$ mm, and $t = 7$ μs (b) at $\varphi_{ch} = 33$ kV.

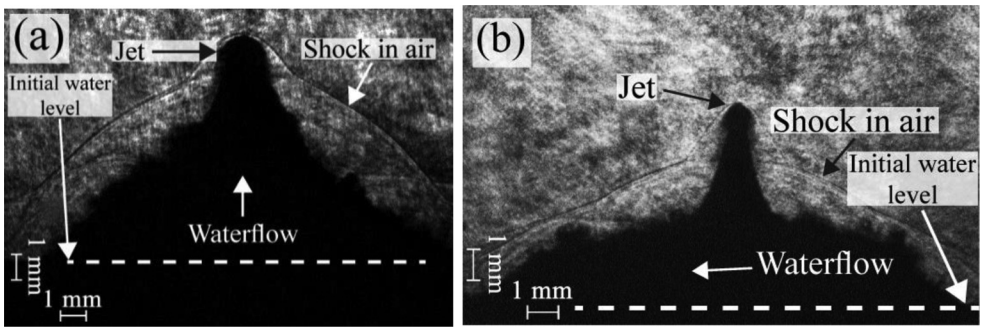

FIG. 4. Shadow images of the waterflow and jet obtained with $d_{ar} = 5$ mm, $h_w = 14$ mm, and $t = 13$ μs (a) and $d_{ar} = 10$ mm, $h_w = 5$ mm, and $t = 13$ μs (b) wire array explosions, at $\varphi_{ch} = 27$ kV.

overtakes the waterflow generated at earlier time at larger radii. This occurs closer to the symmetry axis as compared to $d_{ar} = 10$ mm.

Finally, we carried out explosion experiments at $\varphi_{ch} = 33$ kV for $d_{ar} = 10$ mm, $h_w = 2$ mm, and a cylindrical stainless-steel reflector[21] (14 mm inner diameter, 35 mm long) attached to the grounded electrode of the array [see Fig. 5(b)]. In these experiments, the value of V_w increased to ~1900 m/s. The latter indicates that the application of a reflector leads to an increase in the pressure build-up inside the array due to outgoing shock heading back toward axis.

2. Water jet parameters from cylindrical arrays

Water jets were observed only for $h_w \leq 14$ mm. It is reasonable to associate jet generation with the formation of a high-temperature, dense water-plasma in the vicinity of the implosion axis,[10,11] which is delayed relative to the beginning of the axial waterflow formation (see Fig. 2). The latter is associated with the shock formation and convergences toward the axis. Therefore, the jet, propagating with velocity $V_j > V_w$, overtakes the waterflow at a distance, which is larger than the initial h_w.

As is the case for the waterflow velocity, the jet velocity increases with decreasing h_w. For $d_{ar} = 10$ mm and $\varphi_{ch} = 27$ kV, the jet velocity, V_j, was ~700, ~900, and ~1100 m/s, for h_w ~14, ~10, and ~5 mm, respectively. For the same array and $h_w = 5$ mm, at $\varphi_{ch} = 33$ kV, the value of V_j increased to ~1500 m/s. Also, at $\varphi_{ch} = 33$ kV, decreasing h_w from 5 to 2 mm resulted in the increase in V_j from ~1500 to ~3100 m/s. However, an additional decrease in h_w to 1 mm did not lead to additional increase in V_j, which remained at ~3100 m/s.

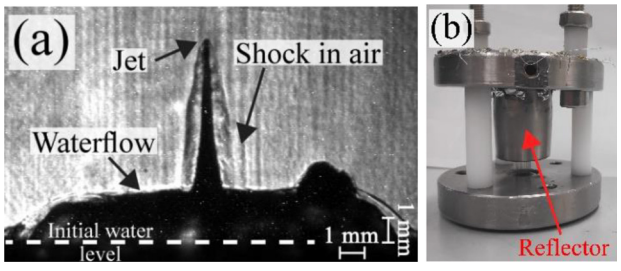

FIG. 5. Typical shadow image of an emerging jet and waterflow for $d_{ar} = 10$ mm and $t = 6$ μs (a) with a reflector (b) and $h_w = 2$ mm. $\varphi_{ch} = 33$ kV.

A decrease in the diameter of the array to 5 mm results in a decrease in the values of V_j. Namely, for $d_{ar} = 10$ and 5 mm array explosions at $\varphi_{ch} = 33$ kV and $h_w = 2$ mm, the jet velocities were ~3100 and ~2600 m/s, respectively. This result, which will be discussed in Sec. IV, was not expected due to the higher energy density which is deposited into the radial waterflow in the case of a 5 mm diameter array explosion.

To decrease the waterflow influence on the jet velocity, namely to allow emerging of the waterflow only at $r \leq 1$ mm, when the remaining time for the shock to reach the axis is ≤0.4 μs, we carried out explosions at $\varphi_{ch} = 33$ kV with $d_{ar} = 10$ mm arrays and $h_w = 1$ mm, when the water/air interface was covered by a collimator. The collimator was made of a 1-mm-thick stainless-steel disk, which has either a 2-mm-diameter hole, or a downward conical (5 mm/2 mm) hole [see Figs. 1 and 6(c)]. This design allows us to decrease the water level to $h_w = 1$ mm without the appearance of sparks, originating from the wire contact with the ground electrode. The results of these shots are summarized in Table I, and typical images of the waterflow and jets are presented in Figs. 6(a) and 6(b). One can see that the application of the cylindrical collimator led to a significant decrease in the value of V_j to ~1800 m/s, which we attribute to a dense waterflow propagating inside the 2-mm-diameter hole. This suggestion agrees with the increased velocity of $V_j \sim 2900$ m/s obtained for a conical collimator. However, this value of V_j is still smaller than for the free water/air interface. We explain this by assuming the formation of a denser radial waterflow inside the array and, consequently, a denser axial waterflow emerging from the conical collimator.

Finally, the results of experiments at $\varphi_{ch} = 33$ kV with $d_{ar} = 10$ mm and $h_w = 2$ mm, with open and covered water surfaces, with a 2-mm-diameter conical collimator, and a stainless-steel reflector are summarized in Table II. One can see that the presence of the reflector alone does not lead to an increase in the value of V_j. However, with both the reflector and collimator, a water jet with a velocity of $V_j \sim 3200$ m/s forms.

B. Generation of water jets by conical wire array explosions

In experiments with explosions of conical arrays (apex angle of $\alpha = 3.57°$) and $h_w = 5$ mm, the jet velocity increases from 1200 m/s to 1700 m/s when the charging voltage was increased from $\varphi_{ch} = 27$ kV to $\varphi_{ch} = 33$ kV. Thus, we performed experiments of conical wire array

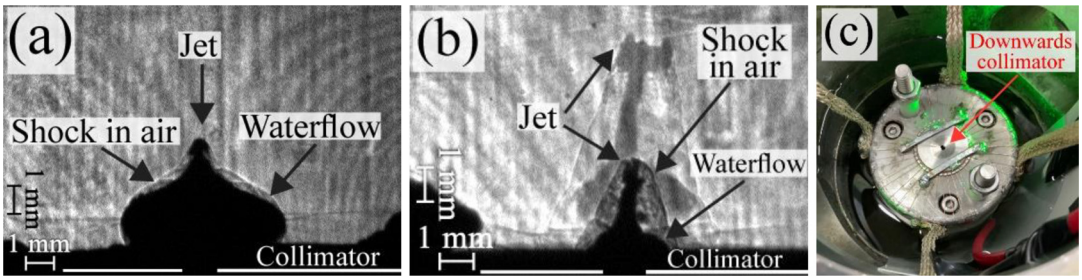

FIG. 6. Shadow image of the emerging jet with a cylindrical collimator, $h_w = 1$ mm, and $t = 5$ μs (a) and an overlapped shadow image of an emerging jet taken 1 μs apart with a conical collimator fitted on a cylindrical array, $d_{ar} = 10$ mm, $h_w = 1$ mm, and $t = 4$ and 5 μs (b). The array is covered with a 2 mm diameter hole downwards conical collimator (c). Both explosions performed at $\varphi_{ch} = 33$ kV. The white lines indicate the borders of the collimator in (a) and (b).

TABLE I. Waterflow and jet velocities obtained in shots with $d_{ar} = 10$ mm cylindrical wire arrays and $h_w = 2$ and 1 mm at $\varphi_{ch} = 33$ kV.

	Waterflow velocity,[a] V_w (m/s)	Jet velocity, V_j (m/s)
Uncovered water layer, $h_w = 2$ mm	1400	3100
Water layer covered with a 2 mm diameter conical collimator, $h_w = 2$ mm	1000	1700
Water layer covered with a 2 mm diameter conical collimator, $h_w = 1$ mm	1700	2900

[a]Here, V_w is the velocity of the waterflow ejected upward from the collimator hole.

TABLE II. Waterflow and jet velocities obtained in explosions of wire arrays with $d_{ar} = 10$ mm and $h_w = 2$ and 1 mm at $\varphi_{ch} = 33$ kV.

	Waterflow velocity, V_w (m/s)	Jet velocity, V_j (m/s)
Open surface of water layer without a reflector	1400	3100
Open surface of water and reflector	1900	3100
Water layer covered by a 2 mm radius conical collimator, reflector present and $h_w = 1$ mm	1800	3200

explosions at $\varphi_{ch} = 33$ kV. For $\alpha = 3.57°$, just like for cylindrical arrays, the velocity of the emerging jet is strongly dependent on the water level. Namely, for water levels $h_w = 5$, 4, and 2 mm the jet velocity was ~1700, ~2700, and ~3200 m/s, respectively. An increase in α to 7.12° has showed a slight decrease in the jet velocity. Namely for the same $h_w = 2$ mm and $\varphi_{ch} = 33$ kV, the jet velocity was ~3000 m/s. Typical shadow images of jets generated in explosions of conical arrays with apexes of 3.57° and 7.12° are shown in Fig. 7.

Next, as in cylindrical array experiments, for $\alpha = 3.57°$ we added a reflector and a 2-mm-diameter conical collimator [see Figs. 5(b) and 6(c)]. Explosions of the array, with a reflector alone and with $h_w = 2$ mm, yielded jet and waterflow velocities of ~3400 and ~1600 m/s, respectively. The use of a conical collimator resulted in the increase in the jet velocity in experiments with $h_w = 1$ mm. In Figs. 8(a) and 8(b), one can see frame and streak images of the waterflow propagating with a velocity of ~2000 m/s and the emerging jet with a velocity of ~3900 m/s. Thus, the application of the collimator and reflector leads to a significant increase in the jet velocity. Let us note a plate-like shape jet head, which was registered only in collimated explosions of arrays (both cylindrical and conical). We assume that this shape can be related to the compressed water layer in the collimator hole, which is accelerated with the jet.

C. Velocity of water jet during propagation in air

A decrease in the jet velocity during its propagation in air was observed for both cylindrical and conical array explosions. Typical dependences of the jet velocities vs the distance are shown in Fig. 9. Using a linear fit of these time-of-flight data, we estimated the maximal average velocity V_j^* of the jet emerging from the cylindrical and conical arrays as ~3450 and ~4450 m/s, respectively.

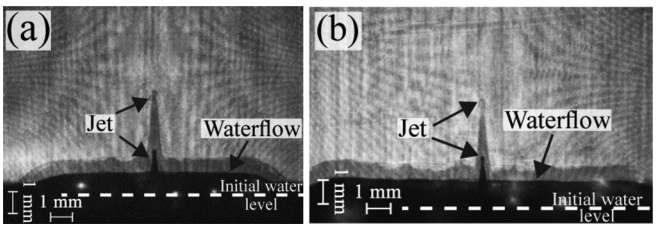

FIG. 7. Overlapped shadow images of the emerging jet in conical wire array explosions with 3.57° apex angle, $h_w = 2$ mm and $t = 4$ and 5 μs (a) and 7.12° apex angle, $h_w = 2$ mm, and $t = 5.5$ and 6.5 μs (b), performed at $\varphi_{ch} = 33$ kV.

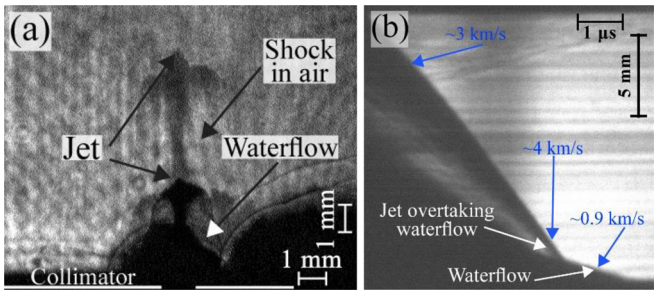

FIG. 8. Overlapped shadow images of an emerging jet for $\alpha = 3.57°$ conical array explosion with a reflector and 2 mm diameter conical collimator, $t = 4$ and 5 μs (a) and the corresponding streak shadow image (b). $h_w = 1$ mm and $\varphi_{ch} = 33$ kV. The white lines indicate the borders of the collimator in (a).

Another estimate of the maximal average velocity V_j^* of the jet emerging from the array was carried out under the assumption that the jet formation occurs at the time when the shock approaches the vicinity of the axis, which correspond to the time of the bright light emission (see Fig. 2). For this approximation, when $\varphi_{ch} = 33$ kV and $h_w = 1$ mm, in explosions of cylindrical and conical arrays with a reflector and conical collimator, the maximal average velocities of the jet were estimated as ~3500 and ~4500 m/s, respectively, which agree satisfactorily with the estimates based on the time-of-flight data.

D. Generation of water jets by aluminum conical array explosions

In an attempt to further increase the jet velocity, several conical array ($\alpha = 3.57°$) explosions, with 40 Al wires, 150 μm diameter, and 35 mm long, at $\varphi_{ch} = 33$ kV, were performed. It was shown[22,23] that using Al wires can lead to a significant increase in the energy delivered to the waterflow, compared to Cu wires, due to Al combustion. In some of these experiments, a reflector was again employed, and the distance between the reflector internal wall and wires was of 2 mm.

In explosions, a critically damped discharge with almost the same parameters as those obtained in explosion of copper wire arrays was realized. For $h_w = 1$ mm and in the presence of a conical collimator and the reflector, waterflow with an extremely high velocity of ~3300 m/s and extensive damage to the collimator was obtained, but without a visible jet. Without the collimator, the velocity of the jet was measured as ~3700 m/s. In Fig. 10, one can see the framing images of the waterflow when the array was fitted with a collimator [Fig. 10(a)] and the emerging waterflow and jet without the collimator [Fig. 10(b)]. Without the collimator, the waterflow below the emerging jet emits a significant amount of light, when compared to experiments with Cu wires for the same water levels, which can be related to Al combustion. We observed that each explosion of the conical Al wire array led to the splitting of the 4-mm-thick reflector into two fractions, which never occurred in Cu wire array explosions. This indirectly indicates that a significant amount of energy was deposited into the waterflow due to Al combustion, which occurs on longer timescales.

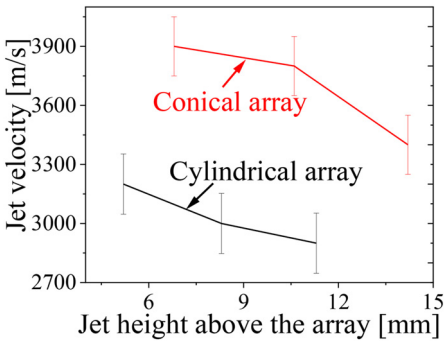

FIG. 9. Average velocity of the jet vs the distance it propagates in air. The jets were generated by explosions of cylindrical and conical arrays fitted with a conical collimator and a reflector where $h_w = 1$ mm and $\varphi_{ch} = 33$ kV.

IV. DISCUSSION

First, we summarize the experimental results in the following list (see also Table III).

- A decrease in the water level above the array for the same values of charging voltage and array geometry leads to an increase in waterflow and jet velocities.
- An increase in the stored energy leads to an increase in the waterflow and jet velocities for explosion of arrays with the same geometry and water level.
- A decrease in the diameter of the cylindrical wire array for the same values of water level h_w and the generator charging voltage, φ_{ch}, leads to a decrease in waterflow and jet velocities.
- An increase in the apex angle of the conical array leads to the decrease in jet velocity.
- Application of a stainless-steel reflector together with a conical collimator does not lead to a significant increase in the jet velocity for explosions of cylindrical arrays.
- The application of a reflector alone leads to an increase in the waterflow velocity.
- For conical array (apex angle of 3.57°) explosions, the application of the reflector and conical collimator led to $V_j \sim 3900$ m/s, the maximal velocity obtained in this research.
- The jet velocity decreases as it propagates in air.
- Explosion of a conical Al array resulted in the increase of the jet velocity as compared to the case of an identical conical Cu wire array when both were fitted with a reflector.

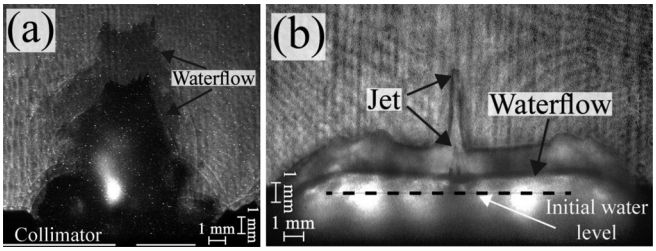

FIG. 10. Overlapped shadow images, 1 μs apart, of the emerging waterflow for $h_w = 1$ mm, $\alpha = 3.57°$ conical Al wire array explosion with a reflector and conical collimator, $t = 6$ and 7 μs (a) and of an emerging jet and light emitting waterflow for the same Al wire array explosion with a reflector but no collimator and $h_w = 2$ mm, $t = 4$ and 5 μs (b). $\varphi_{ch} = 33$ kV. The white lines indicate the borders of the collimator in (a).

TABLE III. Jet velocities for different array configurations. $\varphi_{ch} = 33$ kV.

Array configuration	Application of a reflector and/or conical collimator	Measured jet velocity (m/s)	Estimated jet velocity (m/s)
Cylindrical Cu wire array, $d_{ar} = 10$ mm, $h_w = 2$ mm	Without the reflector and collimator	3100	3900
Cylindrical Cu wire array, $d_{ar} = 10$ mm, $h_w = 2$ mm	With the reflector	3100	4200
Cylindrical Cu wire array, $d_{ar} = 10$ mm, $h_w = 1$ mm	With the reflector and conical collimator	3200	3500[a]
Conical Cu wire array, $d_{ar} = 15/5$ mm, $h_w = 2$ mm	Without the reflector and collimator	3000	3900
Conical Cu wire array, $d_{ar} = 15/5$ mm, $h_w = 2$ mm	With the reflector	3000	4000
Conical Cu wire array, $d_{ar} = 10/5$ mm, $h_w = 2$ mm	Without the reflector and collimator	3200	4100
Conical Cu wire array, $d_{ar} = 10/5$ mm, $h_w = 2$ mm	With the reflector	3400	4700
Conical Cu wire array, $d_{ar} = 10/5$ mm, $h_w = 1$ mm	With the reflector and collimator	3900	4500[a]
Conical Al wire array, $d_{ar} = 10/5$ mm, $h_w = 2$ mm	With the reflector	3700	4800[b]

[a]For a cylindrical array explosion, the collimator could delay the emergence of the jet. This is why we see a "short" jet above the array. This has a smaller effect on conical arrays, which can be explained by the fact that the waterflow behind the shock front has both radial and axial velocity.
[b]Based on estimation of the jet location because the jet was not seen in the first frame, which is screened by the waterflow.

To explain the shape of the waterflow and the timing of the jet we have to consider the formation process. The electrical explosion of wires, accompanied by radial wire expansion, results in the generation of discrete shocks which, upon overlapping, leads to the formation of a symmetric converging shock directed toward the symmetry axis with waterflow behind its front. The velocity of the radial expansion of wires decreases from ~1500 m/s, obtained during the electrical energy deposition, to ~500 m/s within ~6 μs.[10,11] Due to the initial azimuthal distance between neighboring wires (~0.7 and ~0.3 mm for 10 and 5 mm diameter arrays, respectively), overlapping of wires leads to the formation of a cylindrical plasma shell, which forms within several hundreds of ns relative to the beginning of the main energy deposition (see Fig. 2). Assuming an average expansion velocity of ~700 m/s, one obtains that during ~5 μs, the shell should approach radii $\leq$1.5 mm for the 10-mm-diameter array. Note that despite the decrease in the density of the shell, its internal pressure could remain larger than the pressure in the water. Thus, in addition to the shock and waterflow, which approach the axis at $\Delta t \sim 1.8$ and $\Delta t \sim 1.2$ μs for explosions at $\varphi_{ch} = 33$ kV with $d_{ar} = 10$ and 5 mm arrays, respectively, one has to account for how the implosion of the plasma shell, on longer timescales, affects the jet dynamics.

Build-up of the pressure inside the cylindrical plasma shell by the converging waterflow and shell implosion leads to axial waterflow, which is directed toward the open water/air interface with radius dependent velocity. Namely, the velocity of this flow rises with decreasing radius due to the increase in water pressure and density when approaching the axis. At larger radii, the flow, with smaller axial velocity, is generated at earlier times than the flow with larger axial velocity but at smaller radii. Thus, one obtains a time varying concave—flat—convex profile of the waterflow, which agrees with the experimental data (see Fig. 4).

Radial distributions of the pressure, density, and waterflow velocity behind the shock front for different instants of the shock convergence are shown in Fig. 11. These distributions were obtained by one-dimensional hydrodynamic simulations coupled with Equations of State (EOS) for Cu and water,[13–15] for explosions of a Cu wire cylindrical array, 10 mm in diameter, with ~4 kJ deposited energy within ~0.7 μs and time-of-flight of the shock to the implosion axis of ~1.8 μs. One can see a drastic increase in the density, pressure, density, and waterflow velocity in the vicinity of the axis where the temperature increases up to $\geq$2000 °K at $r \leq 10$ μm.

Thus, one can assume that the jet generation occurs in the axis vicinity, where extremely high-pressure axial gradient is realized. In this case, the ejection of the jet from the array occurs through a water "cylinder" which is compressed by the radial waterflow and the converging plasma shell. This time and space dynamic process is difficult to analyze analytically, and two-dimensional hydrodynamic simulations coupled with EOS for copper and water are required, which we plan to carry out. Nevertheless, the results of one-dimensional hydrodynamic simulations can be used for a rough estimate of the jet velocity using energy conservation law as $V_j \approx \sqrt{2P/\rho} \approx 5100\text{m/s}$, where $P \approx 2.8 \times 10^{10}$ Pa and $\rho \approx 2.1 \times 10^3$ kg/m^3 are the pressure and density of water, respectively, in the vicinity of the axis (see Fig. 11). This rough estimate agrees satisfactorily well with the experimental results, indicating the converging shock's symmetry and that the pressure and density in the axis vicinity must be extremely high. However, this estimation approach contradicts experimental results obtained in $d_{ar} = 5$ mm diameter array explosions, when lower velocity of jet was obtained. Indeed, the results of 1D HD simulations showed that one can expect $P \approx 4.6 \times 10^{10}$ Pa and $\rho \approx 2.3 \times 10^3$ kg/m^3, for explosions of a $d_{ar} = 5$ mm array, in the vicinity of the axis. One can consider that because of the viscosity, the jet should decrease its velocity due to friction with the radial waterflow. This qualitative explanation agrees with the results of $d_{ar} = 5$ mm array explosion with a reflector. In this case, an even smaller jet velocity was obtained, in spite of an expected increase in the density and pressure in the vicinity of implosion axis. In addition, for $d_{ar} = 5$ mm array explosion, at ~2.5 μs with respect to the beginning of the discharge current, the cylindrical plasma channel could reach the axis, thus terminating the water jet ejection.

Note that the jet's generation is delayed by Δt relative to the formation of the waterflow ejected in the axial direction from the free surface of the array. For the jet velocity V_j is larger than waterflow velocity V_f, the former will overtake the flow at a distance from the array $Z^* = V_f\left(t - \frac{\Delta Z(t-\Delta t)}{\Delta Z + V_f \Delta t}\right)$, where $\Delta Z = Z_j - Z_w$, Z_w, and Z_j are the distances which the waterflow and jet have reached, respectively, at

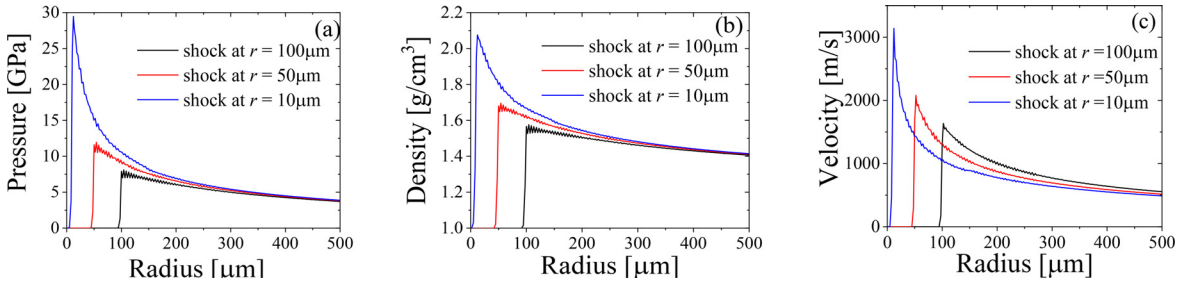

FIG. 11. Radial distributions of the pressure (a), density (b), and waterflow velocity (c) behind the shock front for different times of the shock convergence, simulated for a d_{ar} = 10 mm array.

time t when the shadow image was obtained. Thus, the distance from the array where this overtake occurs grows with larger flow velocities.

The velocity of the waterflow was found to be strongly dependent on the level of water above the array. Namely, for $d_{ar} = 10$ mm at φ_{ch} = 33 kV, this velocity increased from 700 m/s to 2500 m/s when the level of water was decreased from 5 to 1 mm. Taking an average radius of the waterflow of 5 mm and time of ~4 μs (the time interval between the moment of implosion and the time at which shadow images are obtained), one can roughly estimate the kinetic energy of this flow to be $W_k \approx 0.5 V_f^3 \rho \pi r^2 t = 2450$ J. The kinetic energy of the jet estimated in explosions where a $d_{ar} = 10$ mm Cu wire array was used, fitted with a reflector and $h_w = 1$ mm at $\varphi_{ch} = 33$ kV, was ~200 J. Thus, the total kinetic energy of the waterflow and jet can be estimated as 2650 J, which is ~53% of the total energy deposited into the array (see Fig. 2). For these rough estimates, we assumed a water and jet density of 1 g/cm^3, which could be higher, and we neglect the unknown kinetic energy of the downward waterflow from the opposite end of the array (see Fig. 1), or its contribution to the jet velocity at later times. Additional research is required to improve our estimate of the efficiency of the energy transfer to the waterflow and jet. Nevertheless, these estimates indicate that the efficiency of the energy transfer to the waterflow is significantly larger than the ≤24% quoted in earlier studies.[12,13] This apparent difference can be explained by the fact that in earlier studies the efficiency of the energy transfer to the waterflow was calculated only prior to the shock implosion.

The propagation of the jet in air is accompanied by the formation of a shock clearly seen in Figs. 4–6. The velocity of this shock was calculated as $V_{sh} = (h/a)V_j$, where h is the normal distance between the jet surface and the shock front and a is the distance between the jet apex and the slice plane from where the normal to the shock is measured. For instance, explosion of a Cu wire array, with $d_{ar} = 10$ mm at $\varphi_{ch} = 33$ kV, generated a shock with a velocity of ~800 m/s. When the cone apex angle of the jet becomes smaller than $\alpha = \arcsin(M^{-1}) = \arcsin(c_0/V_j)$, one can use this angle to calculate the jet velocity. Here, c_0 is the sound velocity in air and M is the Mach number. Using this approach, in explosions at $\varphi_{ch} = 33$ kV with $d_{ar} = 10$ mm array, fitted with the reflector and $h_w = 2$ mm, we estimated the jet velocity as ~3100 m/s, which agrees well with the time-of-flight measurements.

In array explosions with $h_w = 5$ mm, we have obtained clear signatures of Kelvin–Helmholtz hydrodynamic instabilities,[24] which developed on the side boundaries of the fast propagating jet. For instance, in Fig. 12, one can see two jets propagating in air, generated by an explosion at $\varphi_{ch} = 27$ kV of a cylindrical array with $d_{ar} = 5$ mm [Fig. 12(a)] and 5/10 mm conical array [Fig. 12(b)], both with Cu wires, with measured velocity $V_j \approx 900$ m/s and $V_j \approx 1200$ m/s, respectively. These jets possess typical shape signatures of the Kelvin–Helmholtz instability, where the characteristic length of the visible "teeth" on the side of both jets measured to be ~0.25 and ~0.4 mm, respectively. The results obtained in the present research are not sufficient for conclusions regarding time and space evolution of these instabilities, and additional studies are required.

The results of experiments fitted with the reflector and collimator showed that these allow to achieve even higher jet velocities due to the prevention of reloading of the pressure inside the array by the outward axial and radial waterflows. Also, partial combustion of the Al wire array can be used to further boost the jet velocity, realized by the additional energy transferred to the converging radial waterflow. However, to achieve efficient sub-microsecond timescale combustion, additional research is required, involving a significant increment of the number of Al wires combined with the decrease in the diameter of each wire.[22] Note that it is also worth exploring the explosion of wire array's in different liquids replacing water. For instance, in glycerol, Al wire array explosions could result in additional increase in the jet velocity due to the higher shock velocity because of aluminum and glycerol's possible combustion.[25,26]

Finally, we would like to discuss on the possible mechanisms related to the jet formation. At present, we do not know what phenomenon is responsible for the jet generation and additional research is required. Nevertheless, one can consider jet generation for example, as the result of bubble cavitation.[27–30] For our experimental conditions, formation of a bubble in the vicinity of the water surface cannot

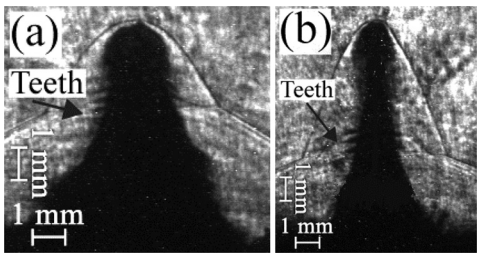

FIG. 12. Shadow frame images of jets generated by the explosion of a $d_{ar} = 5$ mm cylindrical Cu wire array with $h_w = 5$ mm, $t = 16$ μs (a) and 5/10 mm conical Cu wire array with $h_w = 5$ mm and $t = 16$ μs (b) at $\varphi_{ch} = 27$ kV.

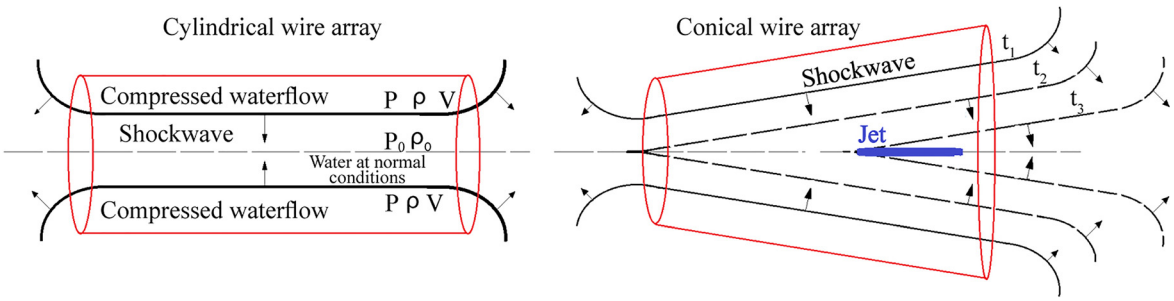

FIG. 13. Qualitative drawings of the compressed waterflow in underwater explosion of cylindrical (left) and conical (right) wire arrays.

be completely excluded. Indeed, implosion of the shock leads to the formation of extreme parameters of water in the vicinity of the implosion axis.[14,15] This state of water may lead to the formation of bubbles. However, we consider this mechanism to be less probable in explaining the jet formation, since it requires creating a bubble close to the water–air interface. This requirement is most likely not fulfilled by our experiments where a jet formed, for water layer thickness of up to ∼14 mm above the array.

The jet formation can also be related to the cumulation effect realized in shaped charges with internal metal conical shells[17] and recently, in an astrophysical problem, where a conical array of wires is electrically exploded in vacuum, resulting in an upward fast plasma jet.[31] Early analytical analysis based on hydrodynamic theory and conservation laws[32,33] predicts jet formation with extremely high velocity, especially when the cone angle approaches zero. However, for a converging conical shock in an ideal gas, jet generation does not occur as predicted.[34,35]

In our experiments, in the vicinity of the axis, the density of water behind the shock front becomes $\geq$2.5 g/cm. Thus, one can consider this flow as an imploding liner, which, at its edges has the funnel-like shape of a front. Qualitative drawings of the possible mechanism of jet formation in explosions of cylindrical and conical wire arrays are presented in Fig. 13. The implosion of this funnel waterflow outside the array, together with the support of dense ($\sim 10^{23}$ cm^{-3}), low-ionized plasma which forms in the vicinity of the implosion axis inside the array, also could explain the jet formation. For a conical wire array, the situation is similar to that described above, with the only difference being, that the implosion of the conical waterflow on the axis of symmetry starts earlier, i.e., inside the array.

This qualitative explanation agrees with the framing shadow image of the jet and shocks generated in air in the case of the conical array explosion (see Fig. 14). One can see that in air, the shock has a funnel shape which corresponds to the propagation of the funnel shape of waterflow at the edge of the array prior to the shock implosion. Implosion of this funnel shaped waterflow could lead later in time to the generation of the jet seen in this frame. For a cylindrical array, we did not obtain such shock in air, probably because of the shorter time interval between the implosion of the funnel waterflow and the jet generation. This qualitative explanation also explains the smaller jet velocity obtained in the explosion of a 5-mm-diameter cylindrical array, compared to the explosion of a 10-mm-diameter cylindrical array, in spite of expecting larger pressure, density and temperature of the water in the vicinity of the axis for the 5-mm case. Indeed, one can expect a decrease in the edge effect with a decrease in the array diameter.

To understand the mechanism responsible for the formation of water jets, we are planning to use synchrotron radiation[36,37] (ERSF, Grenoble, France) to study the jet generation and propagation inside the water layer above the array, where optical diagnostics cannot be used due to the opacity of the compressed water layer through which the jet propagates. Also, we are planning experiments with underwater electrical explosion of a planar wire array(s) to study edge effects, which can be responsible for the formation of the funnel shock front whose implosion could lead to water jet formation.

V. SUMMARY

The experimental results obtained in the current research with a pulse generator operating on the microsecond timescale with a stored energy of <5.7 kJ show that the underwater electrical explosion of cylindrical and conical wire arrays can be used to generate energetic waterflows and jets characterized by a high efficiency (∼50%) of the stored energy transfer to these flows. The time-dependent, radial pressure build-up inside the array, caused by the converging shock and radial expansion of the wires, is responsible for the formation of the axial waterflow with velocities reaching ∼2000 m/s and a corresponding kinetic energy of ∼2500 J. This pressure build-up is also responsible for the formation of an extreme water state in the vicinity of the implosion axis, which, in turn, leads to the generation of the

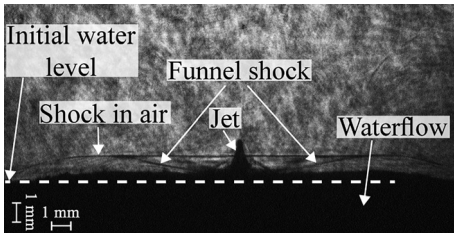

FIG. 14. The shadow image (frame duration of 5 ns) of the waterflow, jet, and shock in air obtained at 6 μs after the beginning of the discharge current with maximum amplitude of ∼340 kA. This underwater electric explosion is for a 5/15 mm conical array with an initial water level of ∼5 mm. The measured jet velocity is ∼2400 m/s and the waterflow velocity is ∼450 m/s.

supersonic axial jet, with average velocities reaching almost ∼5000 m/s and a corresponding kinetic energy of ∼200 J.

Using pulse generators with stored energy of a few tens of kJ, which can be considered as moderate pulse power sources, one can expect the generation of significantly higher energetic waterflows and jets with velocities exceeding >5000 m/s. Such jets can be used in the studies of hydrodynamic instabilities along with the interaction of supersonic jets with different objects and materials.

We also consider to study two such counterstreaming jets generated by the explosion of two conical arrays placed face to face and powered by a single pulse generator. For this case, studies of the interaction of supersonic jets become possible. For this configuration, in the center of mass coordinate system, the velocity of the jet is doubled and the energy of the interacting jet could reach >1 kJ. Owing to the jets' high density ($>10^{22}$ cm^{-3}) and the corresponding high collision rate, one can expect sub-ns-timescale kinetic-energy thermalization leading to the formation of a several eV temperature dense plasma. The latter can be considered a very attractive approach to study the cross-section of the d–d nuclear reaction at ultra-low energies using array explosions in heavy water with jet interaction occurring in a deuterium gas enviroment.[38]

ACKNOWLEDGMENTS

We are grateful to Dr. J. Leopold for fruitful discussions and S. Gleizer, E. Flyat, and R. Samana for technical assistance. This research was supported by the Israel Science Foundation Grant No. 492/18 and in part by the Center for Absorption in Science, Ministry of Immigrant Absorption, State of Israel.

DATA AVAILABILITY

The data that support the findings of this study are available from the corresponding author upon request.

REFERENCES

[1]V. E. Fortov and I. T. Iakubov, *The Physics of Non-Ideal Plasma* (World Scientific, Singapore, 2000).
[2]R. P. Drake, *High-Energy-Density Physics: Fundamentals, Inertial Fusion, and Experimental Astrophysics* (Springer-Verlag, Berlin/Heidelberg, 2006).
[3]J. Larsen, *Foundations of High-Energy-Density Physics: Physical Processes of Matter at Extreme Conditions* (Cambridge University Press, 2017).
[4]S. V. Lebedev, A. Frank, and D. D. Rutov, "Exploring astrophysics-relevant magnetohydrodynamics with pulsed-power laboratory facilities," Rev. Mod. Phys. **91**, 025002 (2019).
[5]D. B. Sinars, M. A. Sweeney, C. S. Alexander, D. J. Ampleford, T. Ao, J. P. Apruzese, C. Aragon, D. J. Armstrong, K. N. Austin, T. J. Awe *et al.*, Phys. Plasmas **27**, 070501 (2020).
[6]L. G. Suttle, G. C. Burdiak, C. L. Cheung, T. Clayson, J. W. D. Halliday, J. D. Hare, S. Rusli, D. R. Russell, E. R. Tubman, A. Ciardi *et al.*, Plasma Phys. Controlled Fusion **62**, 014020 (2020).
[7]A. C. Hayes, M. E. Gooden, E. Henry, G. Jungman, J. B. Wilhelmy, R. S. Rundberg, C. Yeamans, G. Kyrala, C. Cerjan, D. L. Danielson *et al.*, Nat. Phys. **16**, 432 (2020).
[8]L. C. Chhabildas, L. M. Barker, J. R. Asay, T. G. Trucano, G. I. Kerley, and J. E. Dunn, "Launch capabilities to over 10 km/s," in *1991 Proceedings of the APS Topical Conference*, Williamsburg, VA (Elsevier, 1992), pp. 1025–1031.
[9]B. Yu. Sharkov, D. H. H. Hoffmann, A. A. Golubev, and Y. Zhao, Matter Radiat. Extremes **1**, 28 (2016).
[10]Y. E. Krasik, A. Grinenko, A. Sayapin, S. Efimov, A. Fedotov, V. Z. Gurovich, and V. I. Oreshkin, IEEE Trans. Plasma Sci. **36**, 423 (2008).
[11]Y. E. Krasik, S. Efimov, D. Sheftman, and A. Fedotov-Gefen, IEEE Trans. Plasma Sci. **44**, 412 (2016).
[12]A. Grinenko, S. Efimov, A. Fedotov, Y. E. Krasik, and I. Schnitzer, J. Appl. Phys. **100**, 113509 (2006).
[13]S. Efimov, V. T. Gurovich, G. Bazalitski, A. Fedotov, and Y. E. Krasik, J. Appl. Phys. **106**, 073308 (2009).
[14]A. Fedotov Gefen, S. Efimov, L. Gilburd, G. Bazilitski, V. T. Gurovich, and Y. E. Krasik, Phys. Plasma **18**, 062701 (2011).
[15]O. Antonov, L. Gilburd, S. Efimov, G. Bazalitski, V. T. Gurovich, and Y. E. Krasik, Phys. Plasmas **19**, 102702 (2012).
[16]R. H. Cole, *Underwater Explosions* (Princeton University Press, 1948).
[17]W. P. Walters and J. A. Zukas, *Fundamentals of Shaped Charges* (John Wiley & Sons, Inc., 1989).
[18]V. K. Kedrinskii, *Hydrodynamics of Explosion: Experiments and Models* (Springer-Verlag, Berlin/Heidelberg, 2005).
[19]D. Shafer, V. T. Gurovich, D. Yanuka, E. Zvulun, S. Gleizer, G. Toker, and Y. E. Krasik, J. Appl. Phys. **117**, 015901 (2015).
[20]S. Efimov, A. Fedotov, S. Gleizer, V. T. Gurovich, G. Bazilitski, and Y. E. Krasik, Phys. Plasmas **15**, 112703 (2008).
[21]L. Gilburd, S. Efimov, A. Fedotov-Gefen, V. T. Gurovich, G. Bazalitzky, O. Antonov, and Y. E. Krasik, Laser Part. Beams **30**, 215 (2012).
[22]A. Rososhek, S. Efimov, A. Goldman, S. V. Tewari, and Y. E. Krasik, Phys. Plasmas **26**, 053510 (2019).
[23]A. Rososhek, S. Efimov, A. Virozub, D. Maler, and Y. E. Krasik, Appl. Phys. Lett. **115**, 074101 (2019).
[24]T. B. Gatski and J. P. Bonnet, *Compressibility, Turbulence and High Speed Flow* (Academic Press, 2013), pp. 169–230.
[25]D. Yanuka, A. Rososhek, and Y. E. Krasik, Phys. Plasmas **24**, 053512 (2017).
[26]A. Rososhek, S. Efimov, M. Nitishinski, D. Yanuka, S. V. Tewari, V. T. Gurovich, K. Khishchenko, and Y. E. Krasik, Phys. Plasmas **24**, 122705 (2017).
[27]L. Rayleigh, "VIII. On the pressure developed in a liquid during the collapse of a spherical cavity," London, Edinburgh, Dublin Philos. Mag. J. Sci. **34**, 94 (1917).
[28]J. R. Blake and D. C. Gibson, Annu. Rev. Fluid Mech. **19**, 99 (1987).
[29]O. V. Voinov and V. V. Voinov, Sov. Phys. Dokl. **20**, 179 (1975).
[30]T. Li, A.-M. Zhang, S.-P. Wang, S. Li, and W.-T. Liu, Phys. Fluids **31**, 042104 (2019).
[31]S. V. Lebedev, A. Ciardi, D. J. Ampleford, S. N. Bland, S. C. Bott, J. P. Chittenden, G. N. Hall, J. Rapley, C. Jennings, M. Sherlock, A. Frank, and E. G. Blackman, Plasma Phys. Controlled Fusion **47**, B465 (2005).
[32]G. Birkhoff, D. P. MacDougall, E. M. Pugh, and S. G. Taylor, J. Appl. Phys. **19**, 563 (1948).
[33]M. A. Lavrentyev, Achiev. Math. **12**, 41 (1957).
[34]A. I. Rylov, Prikl. Mat. Mekh. **54**, 201 (1990).
[35]H. G. Hornung, J. Fluid Mech. **409**, 1 (2000).
[36]D. Yanuka, A. Rososhek, S. Theocharous, S. N. Bland, Y. E. Krasik, M. P. Olbinado, and A. Rack, J. Appl. Phys. **124**, 153301 (2018).
[37]D. Yanuka, S. Theocharous, S. Efimov, S. N. Bland, A. Rososhek, Y. E. Krasik, M. P. Olbinado, and A. Rack, J. Appl. Phys. **125**, 093301 (2019).
[38]V. M. Bystritsky, V. M. Grebenyuk, S. S. Parzhitski, F. M. Pen'kov, V. T. Sidorov, V. A. Stolupin, T. L. Bulgakov, G. A. Mesyats, A. A. Sinebryukhov, and V. A. Sinebryukhov, Laser Part. Beams **18**, 325 (2000).